ACS APPLIED MATERIALS & INTERFACES

Research Article

www.acsami.org

Improving the Li-Ion Storage Performance of Layered Zinc Silicate through the Interlayer Carbon and Reduced Graphene Oxide Networks

Jin Qu,[†,‡] Yang Yan,[†,‡] Ya-Xia Yin,[†] Yu-Guo Guo,*[,†] and Wei-Guo Song*[,†]

[†]Beijing National Laboratory for Molecular Sciences (BNLMS) & Key Laboratory for Molecular Nanostructures and Nanotechnology, Institute of Chemistry, Chinese Academy of Sciences, Beijing, 100190, P. R. China

[‡]University of Chinese Academy of Sciences, Beijing, 100049, P. R. China

Supporting Information

ABSTRACT: A novel layered zinc silicate/carbon composite was fabricated through carbon embedment into the interlayers of zinc silicate through a hydrothermal method. The interlayer space could be effectively tuned from 1.22 to 3.37 nm by controlling the amount of carbon precursors. Such a layered zinc silicate/carbon structure promoted the lithium ions and electron transportation within the nanostructures, while the reduced graphene oxide (RGO) network improved the conductivity between nanostructures. Such a 3-D carbon based conductive network improved zinc silicates' lithium storage property. After 50 cycles, two composite samples with different carbon loadings showed 778 mA h/g and 704 mA h/g, respectively.

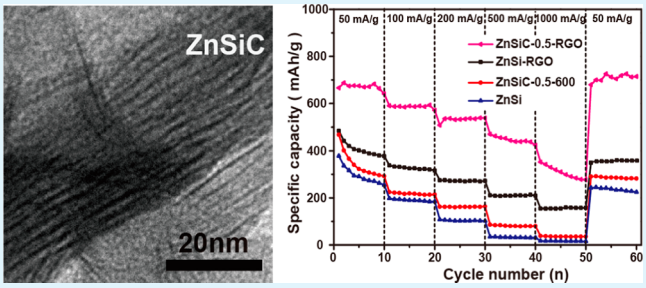

KEYWORDS: *zinc silicate, layered, reduced graphene oxide, 3-D conductive network, Li-ion battery*

INTRODUTION

Layered silicates as an important group of nanomaterials were widely used in adsorption, drug delivery, and catalyst support.[1−7] For example, Song et al. reported 3-D flower-like zinc silicate nanomaterials with layered structures which exhibited a better adsorption capability of lead ions for water treatment.[8] A series of metal silicate nanotubes also showed excellent adsorption capacities of 929 mg/g for uranyl ions and 424 mg/g for lead ions, respectively.[9] However, metal silicates were rarely reported for their electrochemical properties in energy storage devices, as they were usually not conductive. For example, Willemite (Zn_2SiO_4) showed a rapid capacity fading in 20 cycles to 388 mA h/g.[10] Very recently, multiwalled $Ni_3Si_2O_5(OH)_4$ nanotubes used as the anode material in a lithium ion battery were reported to retain a capacity of 226.7 mA h/g after 21 cycles at a rate of 20 mA/g.[11] Such a value was much smaller than conventional graphite (372 mA h/g) and was thus considered as not a useful electrode material.

However, the layered structure of metal silicates is an appealing feature for anode materials in lithium-ion batteries, because such a layered structure provides a well-defined and facile lithium ion transportation route. The only hurdle is the poor conductivity of the metal silicates. Forming composites with carbon nanomaterials is an effective method to advance materials' electrochemical performances in energy storage devices.[12−16] For example, layered MoS_2/amorphous carbon composites have shown much improved electrochemical properties.[17,18] MoS_2 has a layered graphite-like structure, so that carbon could be embedded between the layers by an in situ hydrothermal method. Sandwich-like carbon-supported stacked TiO_2 nanosheets with open channels also showed better electrochemical properties than bulk TiO_2 materials, especially at high rates.[19] Graphene is often integrated with active materials to improve the electrochemical performances in energy storage devices, owing to graphene's excellent electron conductivity, flexibility, chemical stability, and high theoretical surface area (2600 m^2/g).[20−24] Recently, we showed that the layer structured α-Fe_2O_3 constructed with RGO could effectively advance the composites' capacity and cyclability.[25] Thus, we envisioned that if carbon could be inserted into the space between the layers of metal silicates, the composites' lithium ions and electron transportation would be improved in the interlayers. In addition, further addition of reduced graphene oxide would lead to better conductivity between metal silicates.

In this work, we produced a layered zinc silicate/carbon/RGO (ZnSiC-x-RGO, x = 0, 0.5, 1) composite through carbon embedded into the interlayers by a hydrothermal method and then constructed with RGO. The interlayer distance could be effectively tuned from 1.22 to 3.37 nm with an increased amount of glucose as the carbon precursor. Such a layered carbon structure helped the lithium ions and electron

Received: April 10, 2013
Accepted: May 23, 2013
Published: May 23, 2013

   dx.doi.org/10.1021/am401309c | ACS Appl. Mater. Interfaces 2013, 5, 5777−5782

transportation in the interlayers of zinc silicate, while the reduced graphene oxide network improved the electron diffusion between zinc silicate nanoflowers. Such a dual and 3-D carbon based conductive network significantly enhanced the lithium storage property of the composite. After 50 cycles, the composites retained as high as 778 mA h/g for ZnSiC-0.5-RGO and 704 mA h/g for ZnSiC-1-RGO, respectively.

EXPERIMENTAL SECTION

Materials. Analytical-grade zinc chloride, ammonia chloride, $NH_3{\cdot}H_2O$, sodium silicate, NaOH, H_2O_2 (3, 30 wt %), graphite, sulfuric acid, sodium nitrate, $KMnO_4$, and HCl (10 wt %) were purchased from Beijing Chemicals Co. (Beijing, China). Glucose was purchased from Aladdin Chemistry Co. Ltd. All of the chemicals were used as received.

Synthesis of Layered Zinc Silicate/Carbon Composite Nanomaterials (ZnSiC-x, x = 0, 0.5, 1, 2). In a typical procedure, at room temperature, analytical grade zinc chloride (0.75 mmol), ammonia chloride (10 mmol), $NH_3{\cdot}H_2O$ (1 mL), and glucose (0−2 g, samples were named to indicate the content of glucose, e.g. ZnSiC-1g meant 1 g of glucose was used) were mixed in 30 mL of deionized water as solution A; sodium silicate (1.266 mmol) was homogeneously dispersed into 20 mL of deionized water as solution B. The above two solutions were mixed and transferred into a 70 mL autoclave for 12 h at 140 °C. The product was collected by centrifugation and rinsed with distilled water several times. Then, the product was dried in an oven at 60 °C overnight. Finally, the as-prepared samples were heated at 600 or 900 °C for 4 h in a N_2 atmosphere.

Synthesis of Layered Zinc Silicate/C/RGO (ZnSiC-x-RGO, x = 0, 0.5, 1). The layered zinc silicate/carbon/RGO (ZnSiC-x-RGO, x = 0, 0.5, 1) was prepared through dispersing the two materials in an ethanol solution. In a typical procedure: 10 mg of reduced graphene oxide (RGO) was ultrasonicated with 10 mL of ethanol. One hour later, 70 mg of the prepared ZnSiC-x powder was added into the solution under magnetic stirring for 1 h to obtain a homogeneous suspension, then slowly dried at 50 °C. During the solvent vaporization, the ZnSiC-x nanoflowers deposited gradually and embedded into the RGO networks. The final products were dried in an oven at 50 °C for 1 h.

Characterization. The microscopic features of the samples were characterized by scanning electron microscopy (SEM, JEOL-6701F), transmission electron microscopy (TEM, JEOL JEM-1011, 100 kV), and high resolution transmission electron microscopy (HRTEM, JEM 2100F, 200 kV). X-ray powder diffraction (XRD) patterns were collected on an X-ray diffractometer (Rigaku D/max-2500 diffractometer with Cu Kα_1 radiation, λ =1.54056 Å) at 40 kV and 200 mA. The small-angle XRD (SAXRD) measurements were carried out in Rigaku D/max-2400 diffractometer equipped with a secondary graphite monochromator with Cu Kα_1 radiation (λ = 1.5406 Å) at 40 kV and 100 mA. Data were collected in a step-scan mode in the range of 0.6−10° with step-width of 0.02 and speed of 1°/min. Solid-state ^{29}Si and ^{13}C NMR spectra were obtained on an AVANCE III 400 spectrometer using a 7 mm rotor spun at 5 kHz.

Electrochemical Measurements. Electrochemical tests were performed using coin-type cells assembled in an argon-filled glovebox. The working electrode was composed of 80 wt % ZnSiC-x-RGO, 10 wt % super-P, and 10 wt % poly(vinylidene fluoride) (PVDF) or 70 wt % ZnSiC-x-600, 20 wt % super-P, and 10 wt % PVDF and was fabricated by casting a slurry onto a copper foil (99.6%, Goodfellow). The electrolyte was 1 M $LiPF_6$ dissolved in a mixture of ethylene carbonate (EC), dimethyl carbonate (DMC), and diethyl carbonate (DEC) with a weight ratio of 1:1:1 (Tianjin Jinniu Power Sources Material Co., Ltd.). Lithium foil was used as the counter electrodes. A glass fiber (GF/D) from Whatman was used as a separator. Galvanostatic cycling of the assembled cells was carried out using an Arbin BT2000 system in the voltage range of 0.01−3 V (vs Li^+/Li) under a discharge/charge current density of 50−1000 mA/g.

RESULTS AND DISCUSSION

The as-prepared samples showed broad XRD patterns in the range of 10−80° (Figure 1a) that could be indexed to the talc-like structure zinc silicate ($Zn_3Si_4O_{10}(OH)_2{\cdot}nH_2O$).[8] When glucose's amount increased from 0 to 1 g, the intensities of peaks in the range of 10−80° decreased. This indicated that the existence of glucose might change the structure of the crystals during the hydrothermal process. With 2 g of glucose, the original crystal structure was destroyed totally, because all these peaks disappeared. TEM images supported the conclusion. The nanopetal structure and flower-like morphology were retained with glucose up to 1 g (Figure S1a−c). However, the sheet-like nanopetals disappeared, and a pod-like structure appeared while using 2 g of glucose (Figure S1d). Such a pod-like structure by itself might be a novel precursor for fabricating a 1-D ZnO/SiO_2 composite.

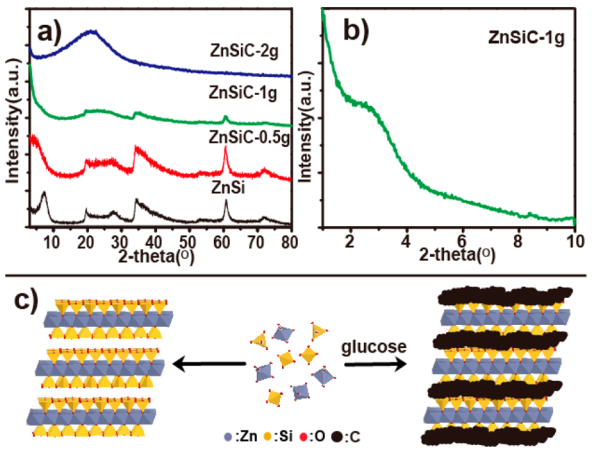

Figure 1. (a) XRD and (b) small angle XRD patterns of the layered zinc silicate/carbon composited nanomaterials before annealing treatment. (c) Schematic illustration of the structure of layered zinc silicate and zinc silicate/carbon composited nanomaterials.

A further analysis in the degree range of lower than 10° to study the layered structure showed the structural difference of the three layered samples' microstructures. As we reported before, there was a strong peak with a 2θ value of 7.22° corresponding to a 1.22 nm interlayer distance when no glucose was added (Figure 1a, black line).[8] Owing to such a large interlayer distance which favored molecules and ions to easily diffuse into layers, it could serve as an ideal host to fabricate composites through physical or covalent modification of interlayers.[26] The layered zinc silicate has an interlayer distance as large as 1.22 nm. Such a large interlayer space favors the transportation of the glucose into the interlayer, and consequent carbonization generates amorphous carbon in situ during the hydrothermal process. Thus, the carbon could be embedded into the interlayers (Figure 1c). With 0.5 g of glucose, the peak shifted to a lower angle around 4.10° corresponding to d = 2.15 nm (Figure 1a, red line). If the content of glucose was increased to 1 g, the peak shifted to much lower angle centered at 2.62° corresponding to d = 3.37 nm, which should be characterized by small angle XRD (Figure 1b). The data indicated that carbon could be sandwiched and the interlayer distance could be effectively tuned through the amount of glucose. The ability to precisely tune the interlayer distance of layered silicate materials allowed us to tailor design

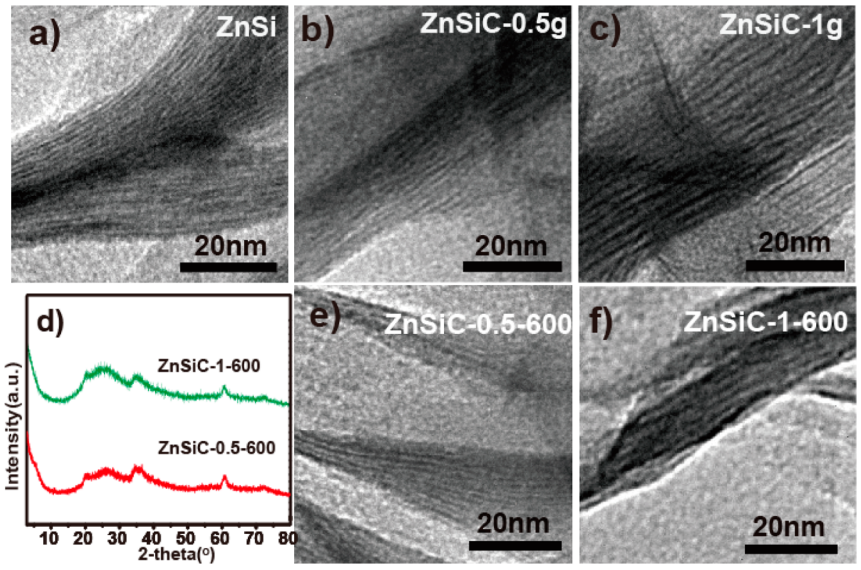

Figure 2. HRTEM images of the layered zinc silicate/C composited nanomaterials: (a) zinc silicate (ZnSi), (b) ZnSiC-0.5g, (c) ZnSiC-1g, (d) XRD patterns and HRTEM images of (e) ZnSiC-0.5-600 and (f) ZnSiC-1-600.

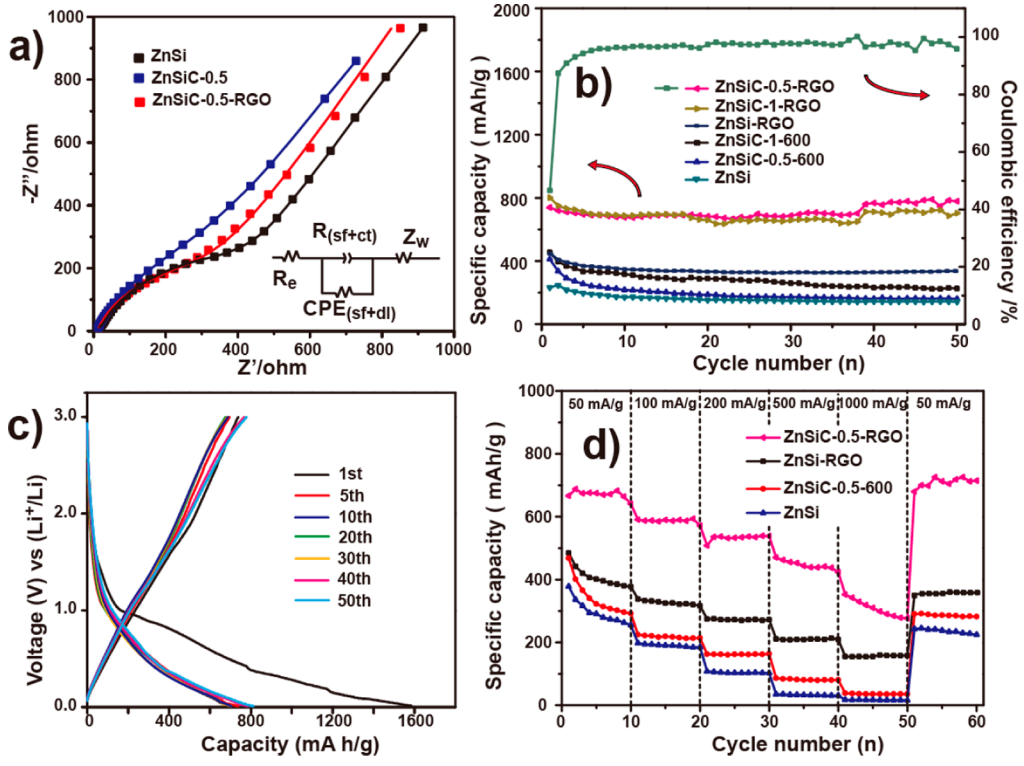

Figure 3. (a) The electrochemical impedance plots of ZnSi, ZnSiC-0.5, and ZnSiC-0.5-RGO without super-P. (b) Cycling performance of the serial electrodes made with ZnSi, ZnSiC-x-600, ZnSiC-x-RGO, and ZnSi-RGO at the current density of 50 mA/g within a voltage window of 0.01−3.0 V. (c) Discharge/charge profiles of ZnSiC-0.5-RGO at first, fifth, 10th, 20th, 30th, 40th, 50th. (d) Reversible charge capacities of the above electrodes cycled at various rates (50−1000 mA/g).

the composite material and investigate the interlayer distance dependent property.

HRTEM images could offer visual layered structures. As shown in Figure 2a−c, the distance between layers expanded while the glucose amount increased. If adding 0.5 g of glucose, the interlayer spacing expanded to 2.15 nm (Figure 2b). With glucose's amount up to 1 g, the interlayer spacing expanded to 3.37 nm accordingly (Figure 2c). Such an interlayer distance increase inferred that carbon was filled into the interlayers through the hydrothermal carbonization process in situ and agreed well with the above XRD results. After annealing treatment at 600 °C in a N_2 atmosphere to improve the carbonization of the glucose-derived carbon, the crystal structure of these composited samples was about the same (Figure 2d) and the layered structure was still retained (Figure 2e,f). After annealing, the interlayer carbon shrunk, and as a result, the interlayer distances decreased to 1.91 nm for ZnSiC-0.5-600 and 2.23 nm for ZnSiC-1-600, respectively. TGA

dx.doi.org/10.1021/am401309c | ACS Appl. Mater. Interfaces 2013, 5, 5777−5782

analysis showed that the weight ratios of carbon were 9% and 23% for ZnSiC-0.5-600 and ZnSiC-1-600, respectively (Figure S3).

The sandwiched carbon not only changed the interlayer distance but also induced the chemical shift change of Si in NMR. The solid state ^{29}Si NMR spectroscopy showed that Q_3 peaks (Q_n referred to Si atoms that connected with n other Si atoms through oxygen bridges, n can be 0−4)[27] shifted from −96.9 ppm for ZnSi to −97.7 ppm for ZnSiC-x-600 (x = 0.5 or 1, Figure S2a). In addition, the solid state ^{13}C NMR spectroscopy showed that the C was mainly in the form of aromatic-C or −CH═CH− in the ZnSiC-x-600 samples (Figure S2b).[28,29] Such amorphous carbon with an sp^2 bond might be effective to improve the composites' conductivity.

As reported, the layered silicates' hollow layer structure was favorable for the insertion and extraction of lithium ions and lithium storage,[11] and 2-D nanosheets could enhance their host capability due to the improved diffusion process upon the intercalation of guest molecules. However, layered silicates' poor conductivity was the main cause for exhibiting a low capacity and a poor cyclability. In this work, the layered carbon formed in situ would enhance the conductivity and then advance lithium ion diffusion and the electron transport process in the interlayers. Lithium ions and electrons could transport deeper through the interlayer carbon in the composite than zinc silicate itself; thus a much higher capacity and cyclability would be expected.

A 3-D conductive network would improve the energy storage property of electrode materials.[13,14] In this study, an elastic reduced graphene oxide (RGO) network was introduced for dispersing, embedding, and electrically wiring the ZnSiC-x nanoflowers while preparing the anode material. RGO combined with the interlayer carbon constructed a novel 3-D carbon based conductive network. The layered carbon structure was expected to be able to improve the conductivity inside the nanoflowers, while the RGO network improved the conductivity between nanoflowers. In order to demonstrate the ability of a 3-D carbon based network to improve the conductivity, bare electrodes (without Super P carbon additive) have been used in measuring the impedance spectra (Figure 3a). The Nyquist plots of the electrodes were constituted by a single depressed semicircle in the high-medium frequency region and an inclined line at low frequency. The experimental data were represented as symbols, and the continuous lines were fitted data according to the equivalent circuit shown in the inset of Figure 3a. The elements in the equivalent circuit include ohmic resistance of the electrolyte and cell components (R_e), surface film resistance (R_{sf}), charge-transfer resistance at the interface between the electrode and electrolyte (R_{ct}), a constant phase element (CPE_i) (sf, double layer (dl)) used instead of pure capacitance due to the depressed semicircle, and Warburg impedance (Z_w). Due to the single semicircle observed, the impedance could be ascribed to the combination of the surface film and charge-transfer resistance $R_{(sf+ct)}$. The fitting parameter of $R_{(sf+ct)}$ was much lower for ZnSiC-0.5-RGO (230 Ω) compared to the ZnSiC-0.5-600 (259 Ω) and zinc silicate alone (339 Ω), which meant that the ZnSiC-0.5-RGO electrode had a more stable surface film (including SEI layer) and faster charge-transfer process than the others. We also measured the impedance spectra of the electrodes with Super-P carbon additive. Their Nyquist plots (Figure S4) showed that the diameter of the semicircle for ZnSiC-x-RGO (x = 0.5 or 1) electrodes in the high-medium frequency region were much smaller than ZnSi alone, confirming that ZnSiC-x-RGO electrodes also possessed much lower contact and charge-transfer resistances with Super-P carbon additive. Thus, we expected that the ZnSiC-x-RGO electrode could possess a high electrical conductivity, a rapid charge-transfer process, and good Li-ion kinetics for lithium uptake and extraction.

The layered zinc silicate/C composites were used as anode materials for lithium-ion batteries, and discharge−charge cycling tests were carried out in the voltage window of 0.01−3 V (vs Li^+/Li) at 50 mA/g and ambient temperature. As expected, the layered composited nanomaterials (ZnSiC-x-RGO) showed significantly higher capacities than zinc silicate alone. Their first charge capacities reached 738 mA h/g for ZnSiC-0.5-RGO and 800 mA h/g for ZnSiC-1-RGO, respectively (Figure 3b, Table S1). Take ZnSiC-0.5-RGO for example: Figure 3c showed that the first discharge capacity was as high as 1586 mA h/g. There was a large irreversible capacity loss and a low initial Coulombic efficiency (ca. 47%) in the first discharge/charge cycle. However, the Coulombic efficiency remained at near 100% in subsequent cycles (Figure 3b). The cyclic voltammogram data of ZnSiC-0.5-RGO (Figure S5) showed that there was a peak at around 0.5 V in the first discharge; then it slightly moved to approximately 0.75 V from the second cycle. This was probably caused by lithium insertion into the interlayers of zinc silicate, which was reversible. After 50 cycles, the capacity of ZnSiC-0.5-RGO increased to 778 mA h/g with cycling whereas the capacity of ZnSiC-1.0-RGO slightly decreased to 704 mA h/g with cycling.

On the basis of the solid state ^{29}Si NMR spectroscopy (Figure S2a), a shoulder peak in the range of −75 to −90 ppm indicated that the coordination state of silica tetrahedrons in the ZnSiC-1.0-RGO was slightly different from the ZnSiC-0.5-600 sample. Such structural change might induce a poor structural stability and capacity fading. The capacity of ZnSiC-0.5-RGO that increased with cycling might be attributed to the improvement of lithium ion accessibility in the hybrid during the cycling processes. However, both values were much higher than that of the zinc silicate alone (144 mA h/g). It indicated that the 3-D conductive network was beneficial to lithium storage. The HRTEM image showed that the layered structure was stable after 50 discharge/charge cycles (Figure S6). It indicated that the composite was stable upon electrochemical galvanostatic cycling, and the intercalation/deintercalation of Li^+ might occur in the interlayers which agreed with reports.[11] As a new anode material, a detailed lithium storage process was unclear. Further detailed investigation is underway. In addition, the ZnSiC-x-RGO's capacities were also much higher than that of the ZnSi-RGO mixture (336 mA h/g), further suggesting that the layered carbons played an important role in enhancing the capacity of the composite.

Recent studies have shown that almost all electrodes, such as Ge@C and α-Fe_2O_3, when composited with RGO, had higher capacities.[14,25] In order to confirm RGO's contribution, the cycling performances of the same ZnSiC-x samples without RGO were also tested under the same conditions. As shown in Figure 3b and Table S1, these initial charge capacities were much lower than the samples containing RGO but still higher than the zinc silicate alone. After 50 cycles, the compared samples retained capacities only 162 or 229 mA h/g for ZnSiC-x-600, while ZnSiC-1-900 had only 42 mA h/g owing to the destroyed layered structure (Figure S7, S8). Thus, both layered carbon and the RGO were essential for the synergistic effect.

The composites also exhibited much improved rate capabilities owing to the novel 3-D conductive network. Take ZnSiC-0.5-RGO for example: Figure 3d showed that it remained at 571 mA h/g, 538 mA h/g, and 424 mA h/g under the current densities of 100 mA/g, 200 mA/g, and 500 mA/g after 10 cycles, respectively. When tested under 1000 mA/g, a decent capacity of 277 mA h/g was still observed for ZnSiC-0.5-RGO, while there were nearly no capacities observed for the zinc silicate alone and the ZnSiC-0.5-600. Although the ZnSi-RGO sample had a relatively good rate performance due to RGO's facilitation, its reversible capacities cycled at various rates (50−1000 mA/g) were much smaller than the ZnSiC-0.5-RGO (Figure 3d). It indicated that the layered carbon was very helpful for lithium storage at high charge/discharge rates.

These excellent properties were credited to the layered structure of the composite, especially the novel 3-D carbon based conductive network. First, such a graphite-like layered structure provided an effective lithium ion transport pathway. Second, the layered carbon allowed much more lithium ions and electron transportation deeper in the composite than zinc silicate itself and then combined with RGO to improve its capacity and cyclability. As shown in Figure 4, which

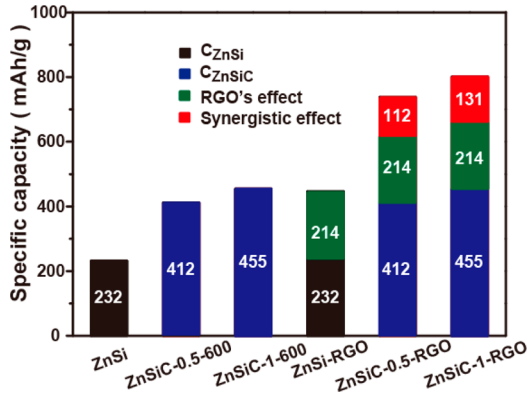

Figure 4. The first reversible charge specific capacity of the ZnSi, ZnSiC-x-600, ZnSi-RGO, and ZnSiC-x-RGO and the calculated specific capacity based on experimental values.

summarized the contribution of each component of the composite, the ZnSiC-x-600 samples had nearly twice higher initial specific capacities than zinc silicate alone, owing to the layered carbon. Besides improving the lithium ion transportation, the layered amorphous carbon might also accommodate lithium ions directly to enhance the overall capacity. However, similar amorphous carbon's specific capacity was less than 200 mA h/g.[17,30] RGO alone could also boost zinc silicate's lithium storage property with a 446 mA h/g capacity, including 214 mA h/g ascribed to RGO's effect. Such a phenomenon was also observed in other reported graphene based composites.[31−33]

However, the capacities of the ZnSiC-x-RGO composite were about 16% higher than the total sum of the individual capacities of ZnSiC-x-600 and RGO's effect, indicating a synergistic effect between these two components. The interlayer amorphous carbon could stabilize the graphene-like zinc silicate nanosheets throughout the cycling process to accommodate more lithium ions, and also keep the active materials electrically connected. And then it combined with RGO providing fast electron transport for ZnSiC-x-600 to improve the lithium storage property. Therefore, the ZnSiC-x-RGO electrodes exhibited significantly enhanced capacities and cyclability. As a result, lithium ion diffusion and electron transfer were also expedited at high rates for the composites. This kind of ZnSiC-x-RGO composite with high capacities and excellent stability would find wide application as promising anode materials for lithium ion batteries.

CONCLUSIONS

In summary, we produced a series of layered zinc silicate/carbon composites through carbon sandwiched in the interlayers by a hydrothermal method in situ. The interlayer distance could be effectively tuned from 1.22 to 3.37 nm through the amount of glucose. Such a layered carbon structure could stabilize the zinc silicate nanosheets throughout the cycling process to accommodate more lithium ions, while the RGO network improved the conductivity between nanoflowers. The layered carbon combined with the RGO constructed an effective 3-D carbon based conductive network to enhance the capacity, cycling performance, and rate capabilities of the composite. After 50 cycles, the composites retained as high as 778 mA h/g for ZnSiC-0.5-RGO and 704 mA h/g for ZnSiC-1-RGO, respectively. The excellent performance of the composite gave evidence for the feasibility of the double carbon enhancement strategy. It also provided us an effective solution to improve the performance of layered nanomaterials in the future.

ASSOCIATED CONTENT

Supporting Information

TEM images of the flower-like zinc silicate/C composite nanomaterials; XRD pattern of the as-prepared samples heated at 900 °C for 4 h in a N_2 atmosphere; the solid state ^{29}Si and ^{13}C NMR spectroscopy of ZnSi, ZnSiC-x, and ZnSiC-x-600; the list of the 1st and 50th cycled charge capacities of the serial samples; cycling performance of the electrode made with ZnSiC-1-900; HRTEM image of as-obtained ZnSiC-0.5-RGO used as the anode material in a lithium ion battery after 50 cycles. This information is available free of charge via the Internet at http://pubs.acs.org/.

AUTHOR INFORMATION

Corresponding Author

*Tel. & Fax: +86-10-82617069 (Y.-G.G.), +86-10-62557908 (W.-G.S.). E-mail: ygguo@iccas.ac.cn (Y.-G.G.), wsong@iccas.ac.cn (W.-G.S.).

Notes

The authors declare no competing financial interest.

ACKNOWLEDGMENTS

We gratefully thank the National Basic Research Program of China (2009CB930400, 2012CB932900), National Natural Science Foundation of China (NSFC 21121063, 51225204), and the Chinese Academy of Sciences (KJCX2-YW-N41) for financial support.

REFERENCES

(1) Martin, J. E.; Patil, A. J.; Butler, M. F.; Mann, S. *Adv. Funct. Mater.* **2011**, *21*, 674−681.
(2) Wang, Y. Q.; Wang, G. Z.; Wang, H. Q.; Liang, C. H.; Cai, W. P.; Zhang, L. D. *Chem.—Eur. J.* **2010**, *16*, 3497−3503.
(3) Wang, Q.; Mynar, J. L.; Yoshida, M.; Lee, E.; Lee, M.; Okuro, K.; Kinbara, K.; Aida, T. *Nature* **2010**, *463*, 339−343.

(4) Wang, X.; Zhuang, J.; Chen, J.; Zhou, K. B.; Li, Y. D. *Angew. Chem., Int. Ed.* **2004**, *43*, 2017−2020.
(5) Komarneni, S.; Kozai, N.; Paulus, W. J. *Nature* **2001**, *410*, 771−771.
(6) Wu, J.; Zhu, Y. J.; Cao, S. W.; Chen, F. *Adv. Mater.* **2010**, *22*, 749−753.
(7) Fang, Q.; Xuan, S.; Jiang, W.; Gong, X. *Adv. Funct. Mater.* **2011**, *21*, 1902−1909.
(8) Qu, J.; Cao, C.-Y.; Hong, Y.-L.; Chen, C.-Q.; Zhu, P.-P.; Song, W.-G.; Wu, Z.-Y. *J. Mater. Chem.* **2012**, *22*, 3562−3567.
(9) Qu, J.; Li, W.; Cao, C.-Y.; Yin, X.-J.; Zhao, L.; Bai, J.; Qin, Z.; Song, W.-G. *J. Mater. Chem.* **2012**, *22*, 17222−17226.
(10) Zhang, S.; Lu, M.; Li, Y.; Sun, F.; Yang, J.; Wang, S. *Mater. Lett.* **2013**, *100*, 89−92.
(11) Yang, Y.; Liang, Q.; Li, J.; Zhuang, Y.; He, Y.; Bai, B.; Wang, X. *Nano Res.* **2011**, *4*, 882−890.
(12) Jiang, K. C.; Xin, S.; Lee, J. S.; Kim, J.; Xiao, X. L.; Guo, Y. G. *Phys. Chem. Chem. Phys.* **2012**, *14*, 2934−2939.
(13) Xin, S.; Guo, Y. G.; Wan, L. J. *Acc. Chem. Res.* **2012**, *45*, 1759−1769.
(14) Xue, D. J.; Xin, S.; Yan, Y.; Jiang, K. C.; Yin, Y. X.; Guo, Y. G.; Wan, L. J. *J. Am. Chem. Soc.* **2012**, *134*, 2512−2515.
(15) Ji, H. X.; Zhang, L. L.; Pettes, M. T.; Li, H.; Chen, S. S.; Shi, L.; Piner, R.; Ruoff, R. S. *Nano Lett.* **2012**, *12*, 2446−2451.
(16) Zhang, K. J.; Han, P. X.; Gu, L.; Zhang, L. X.; Liu, Z. H.; Kong, Q. S.; Zhang, C. J.; Dong, S. M.; Zhang, Z. Y.; Yao, J. H.; Xu, H. X.; Cui, G. L.; Chen, L. Q. *ACS Appl. Mater. Interfaces* **2012**, *4*, 658−664.
(17) Chang, K.; Chen, W. X.; Ma, L.; Li, H.; Li, H.; Huang, F. H.; Xu, Z. D.; Zhang, Q. B.; Lee, J. Y. *J. Mater. Chem.* **2011**, *21*, 6251−6257.
(18) Hwang, H.; Kim, H.; Cho, J. *Nano Lett.* **2011**, *11*, 4826−4830.
(19) Liu, J. H.; Chen, J. S.; Wei, X. F.; Lou, X. W.; Liu, X. W. *Adv. Mater.* **2011**, *23*, 998−1002.
(20) Zhou, X. S.; Yin, Y. X.; Wan, L. J.; Guo, Y. G. *Adv. Energy Mater.* **2012**, *2*, 1086−1090.
(21) Zhou, G. M.; Wang, D. W.; Yin, L. C.; Li, N.; Li, F.; Cheng, H. M. *ACS Nano* **2012**, *6*, 3214−3223.
(22) Luo, B.; Wang, B.; Li, X. L.; Jia, Y. Y.; Liang, M. H.; Zhi, L. J. *Adv. Mater.* **2012**, *24*, 3538−3543.
(23) Zhu, X. J.; Zhu, Y. W.; Murali, S.; Stoller, M. D.; Ruoff, R. S. *ACS Nano* **2011**, *5*, 3333−3338.
(24) Zhang, L. S.; Jiang, L. Y.; Yan, H. J.; Wang, W. D.; Wang, W.; Song, W. G.; Guo, Y. G.; Wan, L. J. *J. Mater. Chem.* **2010**, *20*, 5462−5467.
(25) Qu, J.; Yin, Y. X.; Wang, Y. Q.; Yan, Y.; Guo, Y. G.; Song, W. G. *ACS Appl. Mater. Interfaces* **2013**, *5*, 3932−3936.
(26) Takahashi, N.; Kuroda, K. *J. Mater. Chem.* **2011**, *21*, 14336−14353.
(27) Lippmaa, E.; Maegi, M.; Samoson, A.; Engelhardt, G.; Grimmer, A. R. *J. Am. Chem. Soc.* **1980**, *102*, 4889−4893.
(28) Lundberg, P.; Ekblad, A.; Nilsson, M. *Soil Biol. Biochem.* **2001**, *33*, 621−632.
(29) Webster, E. A.; Chudek, J. A.; Hopkins, D. W. *Biol. Fertil. Soils* **1997**, *25*, 389−395.
(30) Chang, K.; Chen, W. X. *J. Mater. Chem.* **2011**, *21*, 17175−17184.
(31) Yang, S. B.; Feng, X. L.; Ivanovici, S.; Müllen, K. *Angew. Chem., Int. Ed.* **2010**, *49*, 8408−8411.
(32) Yang, S.; Feng, X.; Müllen, K. *Adv. Mater.* **2011**, *23*, 3575−3579.
(33) Zhou, W. W.; Zhu, J. X.; Cheng, C. W.; Liu, J. P.; Yang, H. P.; Cong, C. X.; Guan, C.; Jia, X. T.; Fan, H. J.; Yan, Q. Y.; Li, C. M.; Yu, T. *Energy Environ. Sci.* **2011**, *4*, 4954−4961.